Journal of Molecular Catalysis A: Chemical 345 (2011) 44–53

Contents lists available at ScienceDirect

Journal of Molecular Catalysis A: Chemical

journal homepage: www.elsevier.com/locate/molcata

Effect of zirconium oxide added to Cu/ZnO catalyst for steam reforming of methanol to hydrogen

Yasuyuki Matsumura [a,*], Hideomi Ishibe [b]

[a] National Institute of Advanced Industrial Science and Technology (AIST), Kansai Center, Midorigaoka, Ikeda, Osaka 563-8577, Japan
[b] Nippon Seisen Co. Ltd., Hirakata Plant, Ikenomiya, Hirakata, Osaka 573-8522, Japan

ARTICLE INFO

Article history:
Received 8 September 2010
Received in revised form 25 April 2011
Accepted 22 May 2011
Available online 27 May 2011

Keywords:
Methanol steam reforming
$Cu/ZnO/ZrO_2$
Hydrogen production
Characterization
Deactivation

ABSTRACT

Methanol steam reforming to hydrogen and carbon dioxide is catalyzed over Cu/ZnO prepared by a coprecipitation method. The addition of zirconium ions to the starting material of the catalyst results in improvement of the activity and reduction in the particle sizes of copper and zinc oxide. However, the surface activity of copper on $Cu/ZnO/ZrO_2$ is similar to that for Cu/ZnO. It is suggested that the activity depends mainly on the interaction between Cu and ZnO particles and the presence of zirconium oxide does not directly affect the activity. Steep deactivation occurs over Cu/ZnO in the reaction at 400 °C, but the presence of ZrO_2 particles hampers the aggregation and/or sintering of Cu and ZnO particles and mitigates the deactivation.

1. Introduction

Hydrogen is industrially produced from coal and hydrocarbons such as natural gas and naphtha mainly for desulfurization of petroleum, synthesis of methanol and ammonia, and hydrogenation of chemicals [1]. In recent years hydrogen has been also utilized as the energy resource of fuel cells. Due to environmental issues, polymer electrolyte fuel cells (PEFCs) have gained importance for the automobile industry. However, hydrogen has a problem with its portability, and one of the solutions is on-board hydrogen processing from liquid energy carriers, e.g., methanol, dimethyl ether, and gasoline [2]. Steam reforming of methanol ($CH_3OH + H_2O \rightarrow 3H_2 + CO_2$) is advantageous for the hydrogen production because the reaction usually proceeds over copper catalysts at a reaction temperature lower than 300 °C. Since carbon monoxide poisons the catalytic anodes of PEFCs, the CO content of the hydrogen fuel should be less than 10 ppm [3]. While an extra module for CO removal is required between the reformer and the PEFC unit, the CO selectivity of the methanol steam reforming is significantly small in comparison with the hydrogen production from other liquid energy carriers [2].

In general, $Cu/ZnO/Al_2O_3$ catalysts are used for the reaction due to the high activity and selectivity at low temperatures below 300 °C [4]. However, deactivation easily takes place at a temperature higher than 300 °C [2,5] and the catalysts are not pertinent for a portable hydrogen processor because the reaction temperature often fluctuates and exceeds 300 °C [6,7]. Also, the reactor must be immediately heated up to the reaction temperature under DSS (daily start and stop) operation mode. Thus, the catalyst for the hydrogen processor must be durable against the thermal impact in the reactor. Although copper has a low Tammann temperature, reflecting the low melting point (1083 °C), the thermal stability of Cu/ZnO is often improved by the addition of metal oxides [8]. The methanol steam reforming with $Cu/ZnO/ZrO_2$ has been reported by some researchers and the addition of zirconium oxide generally improves the activity of Cu/ZnO in the reaction at 200–300 °C [9–11]. In the previous study, we found that the $Cu/ZnO/ZrO_2$ ternary catalyst is fairly stable at a reaction temperature as high as 400 °C, but the activity is gradually decreased in the repetition of the reaction [12]. In order to prevent the deactivation, we must understand its mechanism. It was supposed that the presence of zirconium oxide hampers the growth of ZnO particles and the catalytic deactivation is due to the change in the interaction between Cu and ZnO particles [12]. However, Wang et al. reported that the crystalline structure of ZrO_2 affects the activity of Cu/ZrO_2, suggesting the contribution of ZrO_2 to the mechanism [13]. Szizybalski et al. suggested that the activity of Cu/ZrO_2 is affected by the metal-support interaction between Cu and ZrO_2 [14]. Hence, we have characterized the Cu/ZnO and $Cu/ZnO/ZrO_2$ catalysts without deactivation at 250 °C and compared the activities to investigate the effect of zirconium oxide; then, the stability of the catalysts is studied in the reaction at 400 °C.

* Corresponding author. Tel.: +81 72 751 7821; fax: +81 72 751 9623.
E-mail address: yasu-matsumura@aist.go.jp (Y. Matsumura).

1381-1169/$ – see front matter © 2011 Elsevier B.V. All rights reserved.
doi:10.1016/j.molcata.2011.05.017

2. Experimental

Copper supported on zinc oxide (50%Cu/ZnO) was prepared by coprecipitation from a 0.5-M aqueous mixture of $Cu(NO_3)_2{\cdot}3H_2O$ (Wako Pure Chemical, S grade) and $Zn(NO_3)_2{\cdot}6H_2O$ (Wako, S) with addition of an aqueous solution of Na_2CO_3 (0.5 M) under vigorous stirring at 80 °C. After filtration, the precipitate was dispersed in distilled water and washed at room temperature for ca. 0.5 h. The procedure was repeated for several times until the pH value and conductivity of the filtrate reached to the levels of the distilled water. The precipitate was dried at 120 °C for 15 h and finally calcined in air at 500 °C for 12 h. The Cu content was 50 wt.% in the reduced form. The ternary catalyst (40%Cu/ZnO/ZrO_2) was prepared from the same aqueous mixture as for 50%Cu/ZnO except containing $ZrO(NO_3)_2{\cdot}2H_2O$ (Wako, 1st). The Cu and ZnO contents were both 40 wt.% and the ZrO_2 content was 20 wt.%. A commercially available Cu/ZnO/Al_2O_3 catalyst (Süd-Chemie MDC-3) was also used as a reference.

Catalytic tests were performed in a fixed-bed continuous-flow reactor operated under atmospheric pressure. Zirconia balls (1.7 g, 1 mm in diameter) were mixed with a powder catalyst (0.30 g, 50–100 mesh) in order to reduce back pressure during the reaction and keep sufficient length of the catalyst layer. The mixture was placed in a tubular reactor made of stainless steel (i.d., 7 mm) with quartz-wool plugs. In the reaction at 250 °C, the catalyst was pre-reduced at the reaction temperature in a stream of 10-vol.% hydrogen diluted with argon (6.0 $dm^3\ h^{-1}$) for 1 h; then, a reaction mixture of methanol, steam, and argon (1.0/1.2/0.5 in molar ratio) with a flow rate of 29 $dm^3\ h^{-1}$ (F/W, 96 $dm^3\ h^{-1}\ g^{-1}$; methanol feed, 36 $dm^3\ h^{-1}\ g^{-1}$) was admitted. Excess steam was used to reduce the CO by-production and avoid coke formation in the reaction [2]. In the case of Cu/ZnO/Al_2O_3, the catalyst was gradually reduced under the hydrogen stream from 150 °C to 250 °C for 5 h and kept at 250 °C for 1 h because the catalyst is fragile against the overheat in the reduction process [2]. The effluent gas was dried with a cold trap at ca. −50 °C, and analyzed with an on-stream gas chromatograph (Shimadzu GC-8A; activated carbon, 2 m; Ar carrier) equipped with a thermal conductivity detector (TCD). In the reaction at 400 °C, the catalyst was pre-reduced with the reaction mixture at 250 °C for 1 h; then, the reactor was heated up to 400 °C in the reaction flow within 0.3 h for the simulation of the DSS operation. After the reaction, the catalyst was cooled to room temperature under an argon stream. The reaction with 40%Cu/ZnO/ZrO_2 was restarted after heating to 500 °C within 0.5 h in the argon stream in order to give thermal impact. The temperature was kept for 1 h and decreased to 400 °C; then, the reaction was carried out for 7 h and the catalyst was cooled down. The cycle recurred in the following runs.

The methanol conversion was determined from the material balance of the reactant and the products. The error was within 5%. No formation of formaldehyde, methane or methyl formate was observed. The CO selectivity was defined as the molar ratio of CO to that of the sum of CO and CO_2 produced.

Temperature-programmed reduction (TPR) of the catalyst (0.50 g) was carried out in a stream of 10-vol.% hydrogen diluted with argon at a flow rate of 6.0 $dm^3\ h^{-1}$. Temperature of the sample bed was risen linearly at a rate of 200 °C h^{-1}. The hydrogen consumption was monitored by analyzing the hydrogen concentration with the on-stream GC every 3 min. No complete hydrogen consumption was observed in the reduction.

The surface of the sample reduced with hydrogen at 250 °C for 1 h was oxidized by the decomposition of N_2O at 50 °C [15]. After the reduction the sample (0.5 g) was cooled to 50 °C in a flow of helium, and pulses of N_2O were fed. The amount of N_2 produced was measured with a TCD.

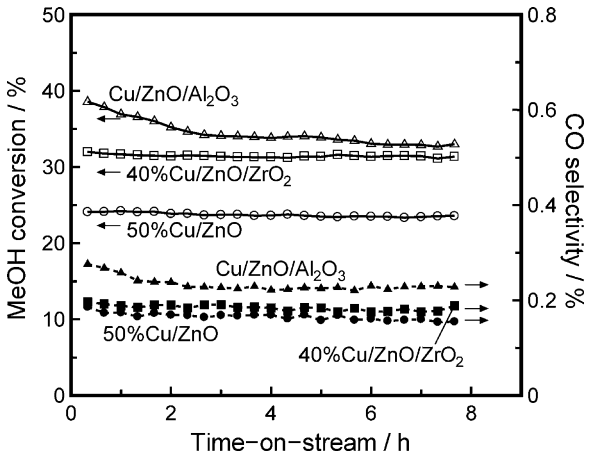

Fig. 1. Catalytic activity of the copper catalysts in methanol steam reforming at 250 °C. Circle symbols, 50%Cu/ZnO; square, 40%Cu/ZnO/ZrO_2; triangle, Cu/ZnO/Al_2O_3. The open symbols show MeOH conversion and the solid symbols show CO selectivity.

The structures of the catalysts after reduction with hydrogen at 250 °C for 1 h were evaluated by transmission electron microscopy (TEM) and high-angle annular dark field imaging in scanning TEM (HAADF/STEM) with energy dispersed X-ray spectroscopic (EDS) analysis using an FEI Tecnai G^2 F20 Twin with an EDX detecting unit (EDAX Inc.) at the acceleration voltage of 200 kV. The EDS analysis was qualitative because the sample was unstable under the electron beam and the data sampling period was limited.

Powder X-ray diffraction (XRD) patterns of the catalysts were recorded in air at room temperature with an MAC Science MP6XCE diffractometer using nickel-filtered Cu Kα radiation.

X-ray photoelectron spectra (XPS) were recorded at room temperature with a JEOL JPS-9010MX spectrometer (Al Kα). The sample reduced with hydrogen at 250 °C for 1 h was mounted to a sample holder under Ar atmosphere and measured without air contact. After the reaction the catalyst sample was taken out from the reactor after cooling under an argon stream for 12 h or longer and mounted in air to a sample holder. Since the sample was gradually oxidized in air, argon spattering (400 V, 7 mA) was carried out for 5 s to remove oxygen adsorbed on the surface. Binding energies were corrected by the reference of the C 1 s line at 284.6 eV. The surface atomic concentrations of Cu, Zn, Zr, and O were calculated from the peak areas using the average matrix relative sensitivity factors (AMRSFs) of Cu $2p_{3/2}$ (32), Zn $2p_{3/2}$ (39), Zr 3d (5.5), and O 1 s (3.4). Since the peak intensity relates to the electron inelastic mean free path of electron for the surface substance, the surface concentrations were corrected using the values of 2.3 nm (Cu) and 2.7 nm (ZnO and ZrO_2) [16]. The AMRSFs were determined by measuring standard materials of Cu, Zn, and Zr metal plates and an alumina plate. The uncertainty of AMRSFs is less than 2% [16].

The BET surface areas of the catalysts were determined from the isotherms of nitrogen physisorption.

3. Results

3.1. Steam reforming of methanol

Steam reforming of methanol to hydrogen and carbon dioxide was carried out over 50%Cu/ZnO at 250 °C after pre-reduction with hydrogen at the same temperature. The methanol conversion with 50%Cu/ZnO was almost stable at 23–24%, and that with a commercial Cu/ZnO/Al_2O_3 catalyst gradually decreased from 39% to 33% for 8 h (Fig. 1). Carbon monoxide was by-produced slightly. Addition of zirconium oxide to Cu/ZnO resulted in increase in the catalytic

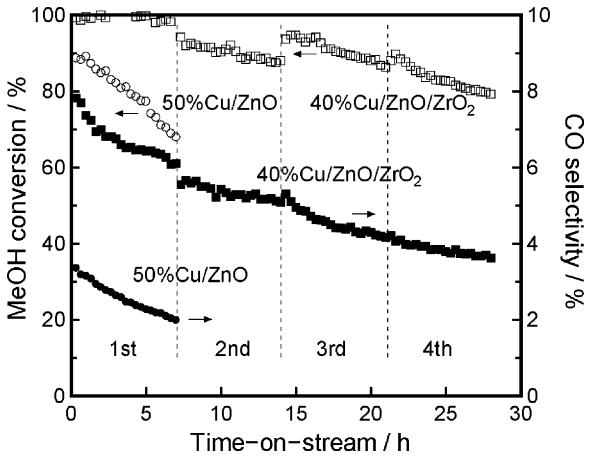

Fig. 2. Catalytic activity of the copper catalysts in methanol steam reforming at 400 °C. Circle symbols, 50%Cu/ZnO; square, 40%Cu/ZnO/ZrO_2. The open symbols show MeOH conversion and the solid symbols show CO selectivity.

activity despite the decrease in the Cu content. The conversion with 40%Cu/ZnO/ZrO_2 was 31–32%. The activity was comparable to that with Cu/ZnO/Al_2O_3 and the CO selectivity was discernibly smaller.

In order to evaluate the stability of the catalysts at a high temperature, steam reforming of methanol was carried out at 400 °C. The activity of 50%Cu/ZnO decreased steeply with an increase in the time period of the reaction, and the CO selectivity also decreased (Fig. 2). The activity of 40%Cu/ZnO/ZrO_2 decreased with the time-on-stream, but the deactivation was gradual in comparison with that observed with 50%Cu/ZnO. The initial activity of the 4th run was almost the same as that of the initial activity of 50%Cu/ZnO, but the final activity was significantly higher than that of the latter. The catalytic activity at the initial stage of the repeated run often increased from the final activity of the previous run. As discussed in the previous paper, the partial restoration of the activity may be due to the change in the surface condition of the catalyst by the pretreatment at 500 °C before the run [12].

3.2. TPR of the Cu catalysts

The reduction of 50%Cu/ZnO started at ca. 110 °C in the TPR experiment (Fig. 3a). The profile showed presence of a couple of peaks and it was deconvoluted into three Gaussian peaks at 146, 167, and 194 °C (Table 1). The molar amount of hydrogen consumption (7.2 mmol g^{-1}) mostly corresponded with the Cu content in the catalyst (7.9 mmol g^{-1}), suggesting that the reduction of CuO particles is nearly completed with the hydrogen consumption for the three peaks. The TPR profile of the 40%Cu/ZnO/ZrO_2 was similar to that of 50%Cu/ZnO (Fig. 3b). The amount of hydrogen consumption was 5.6 mmol g^{-1}, whereas the Cu content was 6.3 mmol g^{-1}.

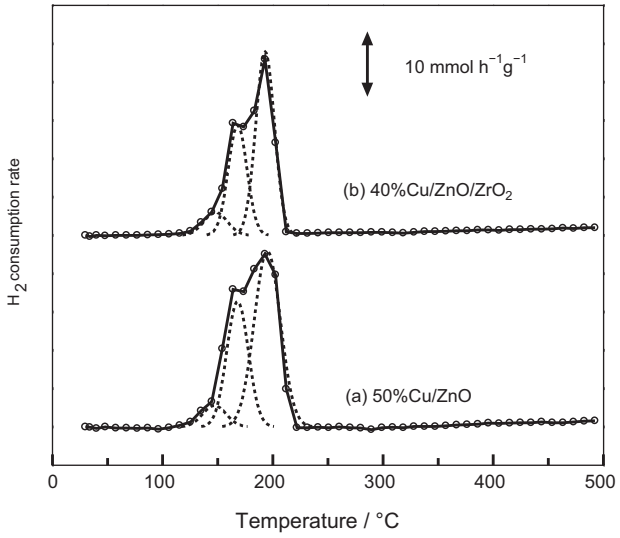

Fig. 3. Profiles of TPR for the copper catalysts with the heating rate of 200 °C h^{-1}. (a) 50%Cu/ZnO and (b) 40%Cu/ZnO/ZrO_2.

Table 1
The amounts of hydrogen consumption in the TPR experiment.

	H_2 consumption, mmol g^{-1} (Temperature, °C)	
	50%Cu/ZnO	40%Cu/ZnO/ZrO_2
Peak 1	0.5 (146)	0.5 (147)
Peak 2	2.5 (167)	1.9 (168)
Peak 3	4.2 (194)	3.2 (192)

In a TPR experiment, 50%Cu/ZnO was reduced up to 170 °C and quenched under an argon stream. The H_2 consumption was 3.0 mmol g^{-1}. When 40%Cu/ZnO/ZrO_2 was reduced up to 170 °C, the H_2 consumption was 2.4 mmol g^{-1}.

3.3. Surface oxidation of the Cu catalysts with N_2O

The quantities of copper on the surface of 50%Cu/ZnO and 40%Cu/ZnO/ZrO_2 reduced with hydrogen at 250 °C for 1 h were evaluated by the surface oxidation with N_2O. The amount of N_2O decomposed on 50%Cu/ZnO was 0.075 mmol g^{-1}. On the basis of the stoichiometry, $2Cu + N_2O \rightarrow Cu_2O + N_2$ [15], the Cu surface area was calculated as 6.2 m^2 g^{-1} where the Cu site density of 0.0243 mmol m^{-2} was assumed. The assumption is commonly used by researchers for measuring the Cu surface area of supported samples [11]. In the case of 40%Cu/ZnO/ZrO_2, the amount of N_2O decomposed was 0.087 mmol g^{-1}, i.e., the Cu surface area was 7.2 m^2 g^{-1}.

3.4. TEM and HAADF/STEM analyses of the Cu catalysts

The HAADF/STEM image of 50%Cu/ZnO reduced with hydrogen at 250 °C for 1 h showed aggregation of particles. Grains whose size was mainly 20–40 nm were observed in the TEM image (Fig. 4a). The Cu particles were not clearly distinguished from ZnO particles in the HAADF/STEM image (Fig. 4b), where the intensity of the image is related to the square of the atomic number (Z^2) of the atoms responsible for the scattering. The EDS analysis (Fig. 4c) showed that the grains at points 2 and 3 were mainly comprised of Cu. On the other hand, Zn was mainly present at points 1 and 4.

The particles in 40%Cu/ZnO/ZrO_2 were also aggregated, but the appearance was significantly different from that for 50%Cu/ZnO. There were two different structures in an aggregate of 40%Cu/ZnO/ZrO_2 as shown in Figs. 5 and 6. Agglomeration of small grains with the size of ca. 5 nm or below was observed with the grains whose size were 10–20 nm (see Fig. 5). The domains were scattered on the surface of the aggregate. Zirconium was detected in parts of the small grains (points 1 and 4) along with Cu and Zn, while Cu and Zn were mainly present in parts of the large grains (points 2, 3, and 5). The agglomeration of small ZrO_2 particles was also observed with other Cu/ZnO/ZrO_2 samples [12]. In the major part of the aggregate, grains with the size of 10–20 nm were mainly present with the small grains which are probably attributed to ZrO_2 (see Fig. 6). At the points 1–5, Cu and Zn were present, and Zr was slightly detected at the points 3–5.

3.5. XRD of the Cu catalysts

Peaks at 35.5°, 38.8°, and 48.7° in 2θ attributed to CuO were recorded with peaks attributed to ZnO in the XRD pattern for

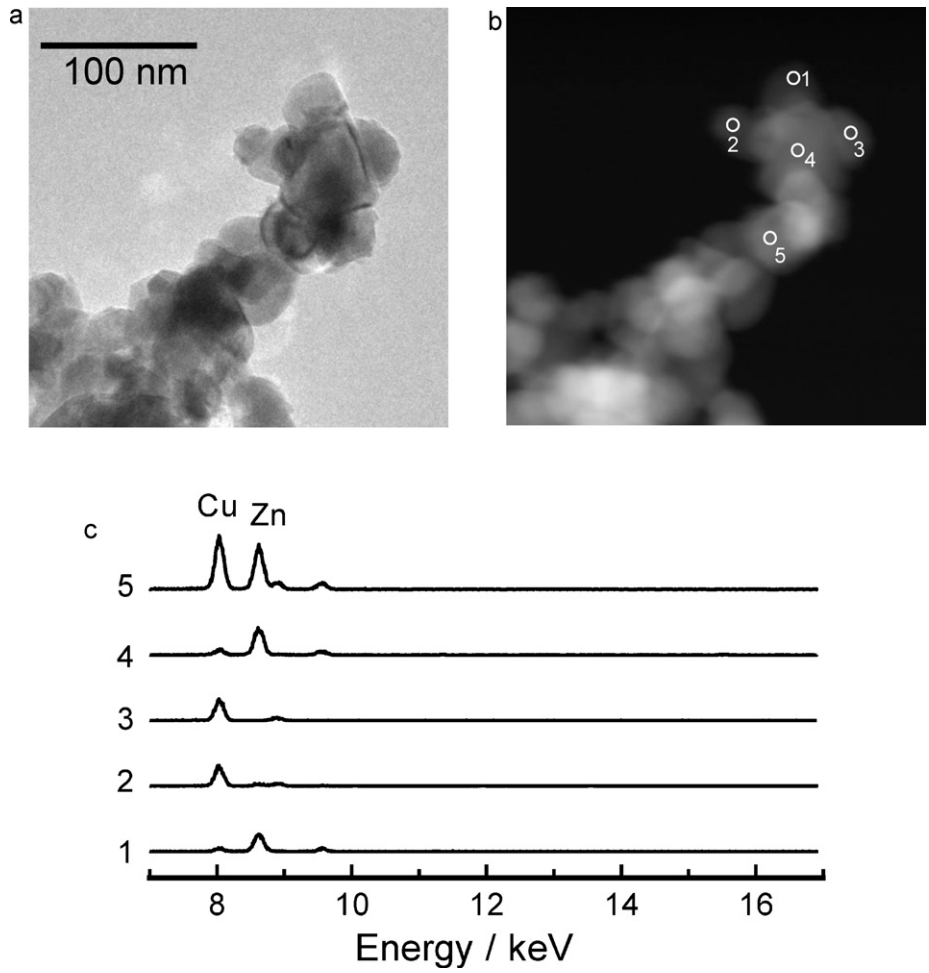

Fig. 4. TEM and HAADF/STEM images and EDS analysis of 50%Cu/ZnO reduced with hydrogen at 250 °C for 1 h. (a) TEM image, (b) HAADF/STEM image, and (c) EDS spectra on points 1–5.

50%Cu/ZnO as prepared (Fig. 7a) [17]. The mean crystallite size of CuO was calculated as 21 nm from the line broadening at 38.8° using Scherrer equation [18], assuming overlapping of two equivalent peaks [CuO(−1 1 1) and CuO(1 1 1)] with the separation of 0.21° [17]. The mean crystallite size of ZnO was 25 nm from the peak at 31.8°.

Peaks at 43.4° and 50.5° being assigned to Cu(1 1 1) and Cu(2 0 0) [17], respectively, appeared with the peaks for CuO in the XRD pattern of 50%Cu/ZnO reduced up to 170 °C in the TPR (Fig. 7b). The mean crystallite size of Cu was 21 nm from the line broadening of Cu(1 1 1) and the size of CuO was 19 nm. The peaks for CuO were completely diminished by the reduction with hydrogen at 250 °C for 1 h and the crystallite size of Cu was 21 nm (Fig. 7c).

No significant peaks attributed to ZrO_2 were recorded in the XRD pattern for 40%Cu/ZnO/ZrO_2 as prepared (Fig. 8a). The mean crystallite sizes of CuO and ZnO were both 14 nm. The peaks attributed to metallic Cu appeared with the peaks for CuO in the pattern of the sample reduced up to 170 °C in the TPR (Fig. 8b). The mean crystallite size of Cu was 14 nm and the size of CuO was 17 nm. The peaks for CuO were completely diminished by the reduction with hydrogen at 250 °C for 1 h and the crystallite size of Cu was 14 nm (Fig. 8c). As can be seen in Fig. 5, there were small ZrO_2 particles with the size of 5 nm or below in the sample, but the intensity of the peak at ca. 30° attributed to ZrO_2 was very weak [17]. Thus, the small ZrO_2 particles were amorphous and undetectable by XRD [12].

The peaks attributed to Cu metal were recorded in the XRD pattern of a different aliquot of 50%Cu/ZnO taken out from the reactor after the reforming at 400 °C for 0.5 h (not shown). No peaks attributed to CuO were observed. The mean crystallite size of Cu was calculated as 28 nm and that of ZnO was also 28 nm. The size of Cu after the run for 7 h was 26 nm. The mean crystallite sizes for the catalysts were summarized in Table 2.

A small peak attributed to tetragonal ZrO_2 appeared at 30.5° in the pattern for 40%Cu/ZnO/ZrO_2 after the reaction at 400 °C for 0.5 h (Fig. 9a), and the peak was gradually intensified with the time period of the reaction (Fig. 9b and c). The crystallite size of Cu for 40%Cu/ZnO/ZrO_2 after the 1st run was 20 nm and significantly

Table 2
Mean crystallite sizes of the catalysts after the reaction at 400 °C. The sizes were determined from the XRD peaks of Cu(1 1 1), Zn(1 0 0), and ZrO_2(1 1 1).

Catalyst	Time-on-stream, h	Mean crystallite size, nm		
		Cu	ZnO	ZrO_2
50%Cu/ZnO	Reduced[a]	21	21	–
50%Cu/ZnO	0.5	28	28	–
50%Cu/ZnO	7	26	28	–
40%Cu/ZnO/ZrO_2	Reduced[a]	14	14	6
40%Cu/ZnO/ZrO_2	0.5	20	14	9
40%Cu/ZnO/ZrO_2	7	21	16	10
40%Cu/ZnO/ZrO_2	7 × 4	24	28	10

[a] Just after reduction with hydrogen at 250 °C for 1 h.

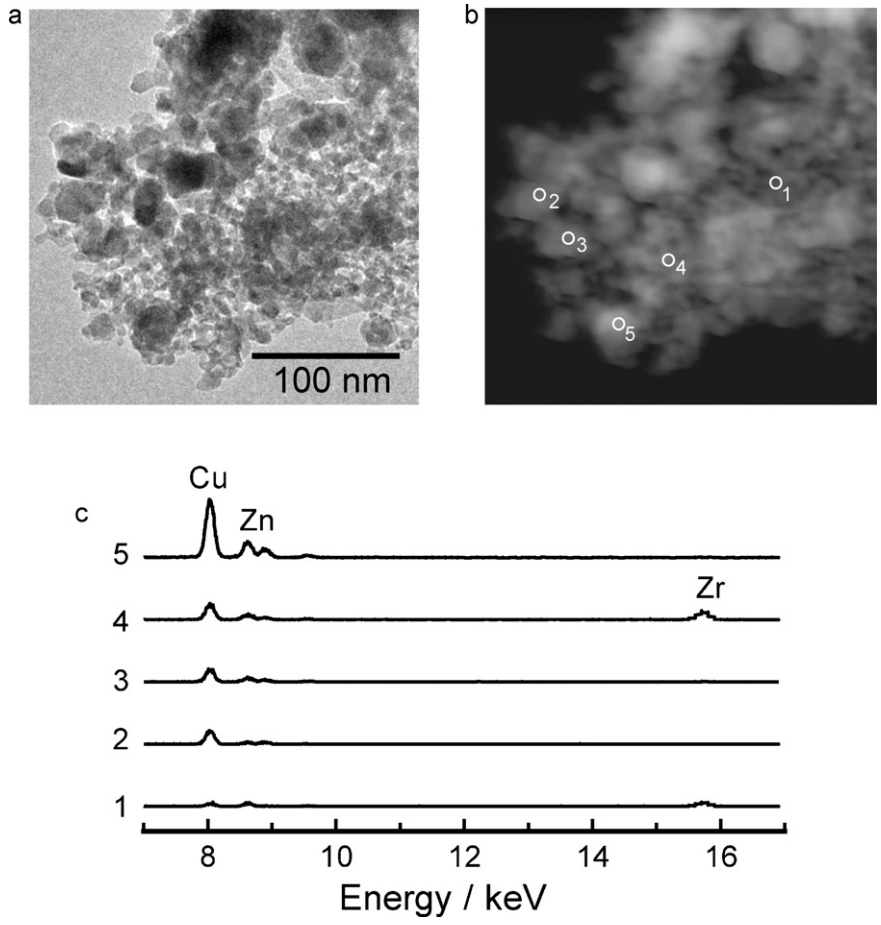

Fig. 5. TEM and HAADF/STEM images and EDS analysis of 40%Cu/ZnO/ZrO_2 reduced with hydrogen at 250 °C for 1 h. (a) TEM image, (b) HAADF/STEM image, and (c) EDS spectra on points 1–5.

smaller than that for 50%Cu/ZnO. The size increased to 24 nm after the 4th run. The size of ZnO increased significantly from 14 nm after the reaction for 0.5 h to 28 nm after the 4th run.

3.6. XPS of the Cu catalysts

The surface of the copper catalyst was characterized by XPS. The binding energy of Cu $2p_{3/2}$ was 932.2 eV for 50%Cu/ZnO reduced with hydrogen at 250 °C for 1 h, and the energy for 40%Cu/ZnO/ZrO_2 was 932.4 eV (Fig. 10). Since the binding energies were close to those for Cu metal (932.67 eV) and Cu_2O (932.4 eV) [19], the Auger line of Cu L_3VV was recorded to identify the oxidation state. The kinetic energies for 50%Cu/ZnO and 40%Cu/ZnO/ZrO_2 were 919.0 and 918.8 eV, respectively (Fig. 11), whereas the energies for Cu metal and Cu_2O are 918.65 and 916.8 eV, respectively [19]. The α values (Auger parameter + photon energy) for 50%Cu/ZnO and 40%Cu/ZnO/ZrO_2 were both 1851.2 eV, showing that the surface species are metallic; the value for metallic Cu is 1851.3 eV [19]. The binding energies of Zn $2p_{3/2}$ for 50%Cu/ZnO and 40%Cu/ZnO/ZrO_2 were both 1021.8 eV. The kinetic energies of Zn $L_3M_{45}M_{45}$ were both 988.4 eV (α value, 2010.2 eV), whereas the α value for ZnO is 2009.8 eV [19]. The binding energies of O 1 s were both 530.5 eV and the energy of Zr $3d_{5/2}$ for 40%Cu/ZnO/ZrO_2 was 182.1 eV.

The surface atomic concentrations of Cu for 50%Cu/ZnO taken out after the reaction at 400 °C for 0.5 and 7 h were 14% and 16%, respectively (Table 3). The surface concentrations of Cu for 40%Cu/ZnO/ZrO_2 after the reactions at 400 °C were smaller than those of 50%Cu/ZnO. The concentration of Zn^{2+} decreased significantly after the 4th run and that of Zr^{4+} increased reversely. The binding energy of Cu $2p_{3/2}$ was 932.2–932.6 eV regardless

Table 3
Surface atomic concentrations determined by XPS and BET surface areas of the catalysts after the reaction at 400 °C.

Catalyst	Time-on-stream, h	Surface atomic concentration, %			BET surface area, $m^2\,g^{-1}$	Cu surface quantity,[b] $mmol\,g^{-1}$
		Cu	Zn^{2+}	Zr^{4+}		
50%Cu/ZnO	Reduced[a]	18	24	0	26	0.16
50%Cu/ZnO	0.5	14	27	0	17	0.08
50%Cu/ZnO	7	16	19	0	14	0.07
40%Cu/ZnO/ZrO_2	Reduced[a]	10	15	13	60	0.21
40%Cu/ZnO/ZrO_2	0.5	10	17	14	31	0.11
40%Cu/ZnO/ZrO_2	7	12	16	13	27	0.12
40%Cu/ZnO/ZrO_2	7 × 4	12	11	17	28	0.12

[a] Just after reduction with hydrogen at 250 °C for 1 h.
[b] The quantity was calculated from the surface atomic concentrations and BET surface area.

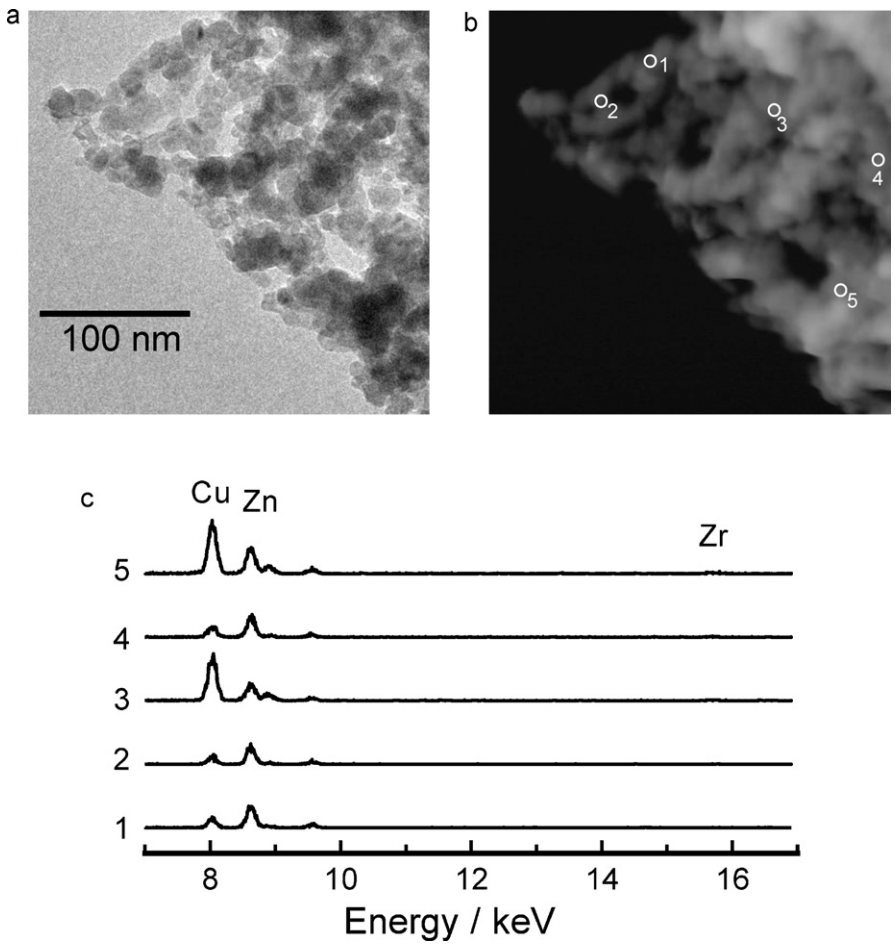

Fig. 6. TEM and HAADF/STEM images and EDS analysis of a different portion in the same aggregate of 40%Cu/ZnO/ZrO_2 shown in Fig. 5. (a) TEM image, (b) HAADF/STEM image, and (c) EDS spectra on points 1–5.

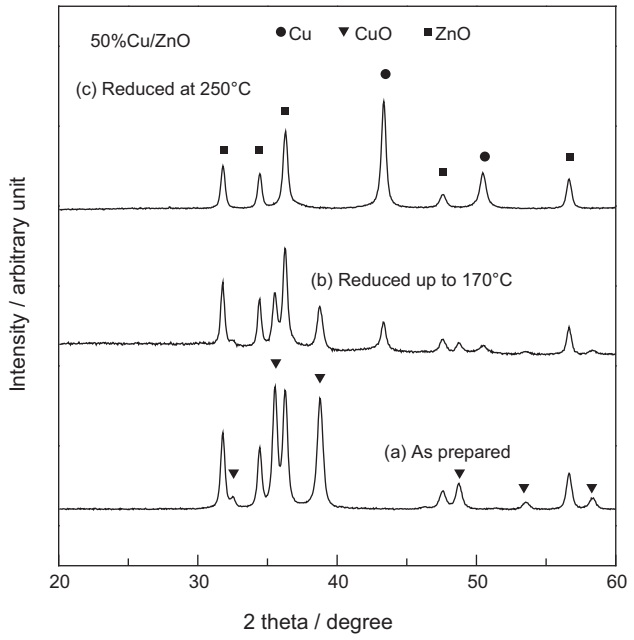

Fig. 7. XRD patterns of the 50%Cu/ZnO. (a) As prepared, (b) reduced up to 170 °C in TPR, and (c) reduced with hydrogen at 250 °C for 1 h.

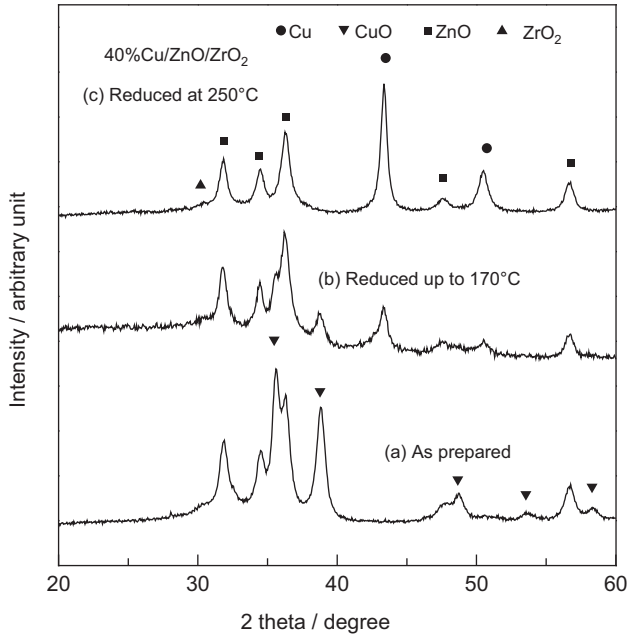

Fig. 8. XRD patterns of the 40%Cu/ZnO/ZrO_2. (a) As prepared, (b) reduced up to 170 °C in TPR, and (c) reduced with hydrogen at 250 °C for 1 h.

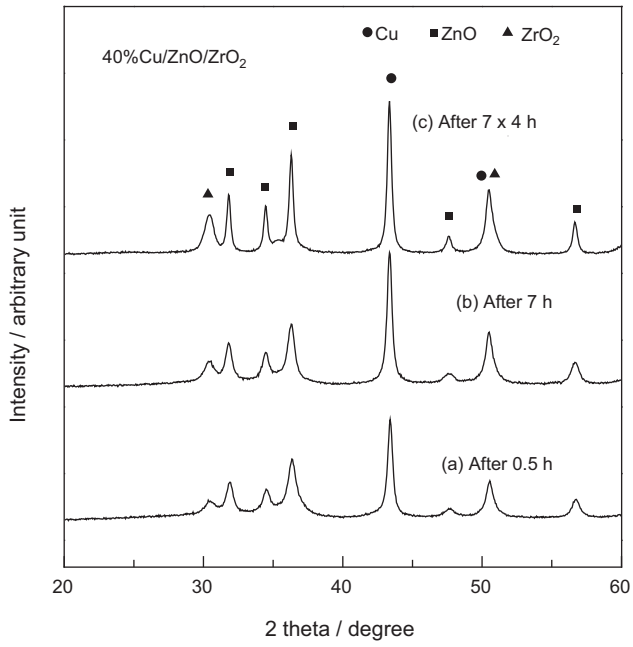

Fig. 9. XRD patterns of 40%Cu/ZnO/ZrO_2 after the reaction at 400 °C. (a) After 0.5 h-on-stream, (b) after 7 h-on-stream, and (c) after the 4th run.

of the samples. The kinetic energy of Cu L_3VV (Auger line) was 918.5–919.1 eV and the α value (Auger parameter + photon energy) was 1851.1–1851.4 eV, showing copper on the surface was reduced to metal by the sputtering. The binding energies were 1021.7–1021.8 eV for Zn $2p_{3/2}$, and 530.2–530.6 eV for O 1 s regardless of the samples. The binding energies of Zr $3d_{5/2}$ for 40%Cu/ZnO/ZrO_2 after the reactions were 182.2–182.4 eV.

3.7. BET surface area of the Cu catalysts

The BET surface area of 50%Cu/ZnO was 26 $m^2\,g^{-1}$ after the reduction with hydrogen at 250 °C and that for 40%Cu/ZnO/ZrO_2 was 60 $m^2\,g^{-1}$ (see Table 3). After the reaction at 400 °C for 0.5 h, the surface area for 50%Cu/ZnO was 17 $m^2\,g^{-1}$ and it decreased

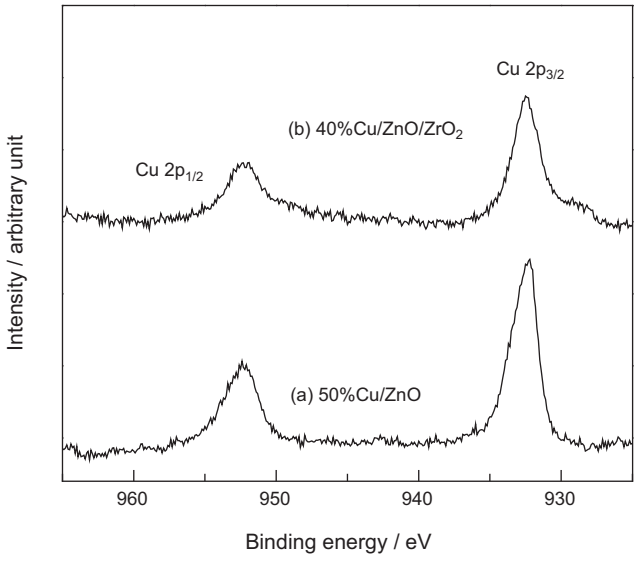

Fig. 10. XPS of Cu 2p region for the Cu catalysts reduced with hydrogen at 250 °C for 1 h. (a) 50%Cu/ZnO and (b) 40%Cu/ZnO/ZrO_2.

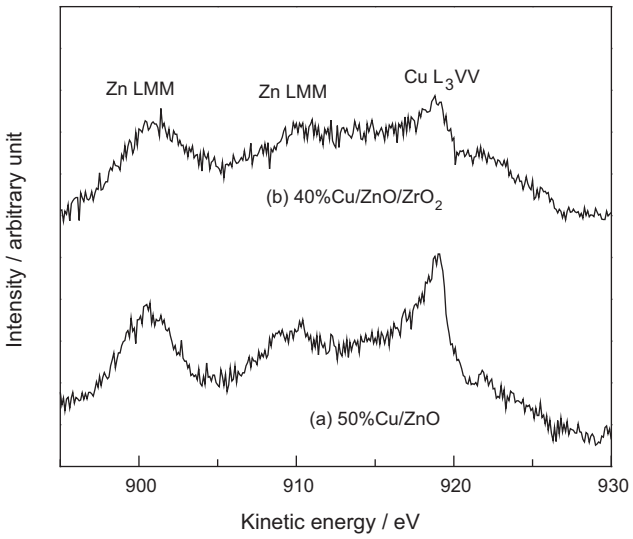

Fig. 11. Auger line of Cu L_3VV for the Cu catalysts reduced with hydrogen at 250 °C for 1 h. (a) 50%Cu/ZnO and (b) 40%Cu/ZnO/ZrO_2.

to 14 $m^2\,g^{-1}$ after 7 h-on-stream. On the other hand, the areas for 40%Cu/ZnO/ZrO_2 in the reaction at 400 °C were 27–31 $m^2\,g^{-1}$.

4. Discussion

4.1. Morphology of the Cu catalysts

The addition of zirconium oxide to Cu/ZnO significantly increases the surface area and it is generally observed by other researchers [9–11]. While the presence of small ZrO_2 particles should contribute to the greater surface area, the sizes of Cu and ZnO are decreased in the presence of zirconium oxide as evidenced by the TEM images (see Figs. 4–6) and XRD (see Table 2). Hence, the addition of zirconium oxide results in the higher dispersion of Cu and ZnO particles and it also contributes to the greater surface area [12].

Since the BET surface area of 50%Cu/ZnO is 26 $m^2\,g^{-1}$ and the Cu surface area determined by the N_2O adsorption is 6.2 $m^2\,g^{-1}$, the actual surface area of ZnO will be 20 $m^2\,g^{-1}$. Assuming that all the ZnO particles are spherical and the whole surface is exposed, the particle size is calculated as 26 nm from the area. Since the particle size observed by TEM is mainly 20–40 nm and the mean crystallite size of ZnO is 21 nm, which is often close to the mean particle size [20,21], it is estimated that most of the ZnO particle surface is exposed; the surface area of ZnO is calculated as 25 $m^2\,g^{-1}$ when the particle size is 21 nm. On the other hand, the size of Cu particles is calculated as 54 nm from the Cu surface area, assuming that the whole surface is exposed. However, the particles seen in TEM are mostly smaller than the size and the mean crystallite size of Cu is 21 nm. If the Cu particles are spherical with a diameter of 21 nm, the surface area of the particles will be 16 $m^2\,g^{-1}$. This suggests that a significant part of the Cu surface is covered with other particles. Kasatkin et al. evidenced surface adhesion of Cu particles on the surface of zinc oxide by the TEM measurement [22,23]. Fig. 4 also shows that Cu and ZnO particles in 50%Cu/ZnO are mixed and have the surface contact. Hence, it is estimated that Cu particles interacts strongly with ZnO particles. On the basis of the Cu surface area for 40%Cu/ZnO/ZrO_2, the Cu particle size is calculated as 37 nm. The size is significantly larger than the Cu crystallite size of 14 nm, and the particle size seen in the TEM is mostly 20 nm or less. This suggests that the surface of Cu particles in 40%Cu/ZnO/ZrO_2 is also considerably covered with ZnO and/or ZrO_2 particles.

A couple of TPR peaks often appear with ZnO and/or ZrO_2-supported copper catalysts which are prepared by the coprecipitation method [10,11,24–26]. In general the peak position depends on the size of CuO particles and the small particles are usually reduced at a low temperature [27,28]. However, the peak positions for 50%Cu/ZnO are almost the same as those for 40%Cu/ZnO/ZrO_2 (see Fig. 3 and Table 1) although the Cu particle size for 50%Cu/ZnO is significantly larger than that of the latter. In addition, no significant difference in the mean crystallite size of Cu is observed between the samples after the reduction up to 170 °C and 250 °C, showing that the reduction temperature does not depend obviously on the particle size. It is known that the reduction temperature of CuO decreases in the presence of a small amount of ZnO, but the temperature does not change significantly with increasing the ZnO content [24]. Kurr et al. reported absence of the high temperature peak in the TPR of Cu/ZnO/Al_2O_3 when the Cu surface area determined by N_2O absorption was close to that calculated from the XRD line broadening [29]. This suggests that the CuO particles whose surface is mostly exposed are easily reduced. Hence, it is probable that the high temperature peak is due to the reduction of the CuO particles whose surface is greatly covered with other oxide particles. It is supposed that these CuO particles are mainly encapsulated in the aggregation. Günter et al. reported the formation of Cu_2O at the initial stage of the TPR for Cu/ZnO [30], suggesting that the reduction at low temperature is partly due to the partial reduction of the exposed CuO particles to Cu_2O.

4.2. Activity of the Cu catalysts in the reaction at 250 °C

It was reported that the turnover frequency (TOF) of Cu/ZnO to the methanol steam reforming at 220 °C does not depend simply on the Cu surface area [31]. It is discussed that the structural disorder of Cu particles increases the activity to methanol steam reforming [30,32]. Since the disorder is due to the surface interaction between Cu and ZnO particles, the particle sizes and the geometry should affect the activity. In the case of 40%Cu/ZnO/ZrO_2, the surface structure is inhomogeneous as shown in Figs. 5 and 6. However, Cu is usually detected with Zn in the EDS analysis, suggesting that most of Cu particles are in contact with ZnO particles while the interaction with ZrO_2 particles cannot be excluded. Since the ZrO_2-rich domains are partly present on the surface of the aggregate, it is supposed that excessive zirconium oxide forms the domains and the major part of Cu and ZnO particles forms the structure shown in Fig. 6 where the population of ZrO_2 is small.

In the case of 50%Cu/ZnO, the TOF at 250 °C is calculated as 0.66 s^{-1} from the initial methanol conversion and the surface quantity of copper atoms determined by the N_2O adsorption. The TOF for 40%Cu/ZnO/ZrO_2 is 0.76 s^{-1}, showing that the addition of ZrO_2 does not greatly improve the activity of Cu surface. Since the methanol conversion below ca. 30% is approximately in proportion to W/F (contact time) [33], at least one significant figure of the TOF is reliable. Agrell et al. reported that the TOFs of 38 wt.% Cu/ZnO and 27 wt.% Cu/46 wt.% ZnO/32 wt.% ZrO_2 are 0.10 and 0.21 s^{-1} at 250 °C, respectively, where the Cu surface areas are 20.8 and 15.5 $m^2\ g^{-1}$, respectively [10]. The TOFs are significantly lower than ours even if taking into consideration of the difference in the reaction conditions, e.g., their high F/W of 276 $dm^3\ g^{-1}$ and low methanol feed of 23 $dm^3\ g^{-1}$. In general, the higher F/W produces the higher TOF because the methanol conversion is gradually saturated with a decrease in F/W. On the other hand, the lower methanol feed results in the reduction of the TOF. In the present study, the methanol feed is 36 $dm^3\ g^{-1}$. If the TOF is in proportion to the methanol feed, the TOFs for Cu/ZnO and Cu/ZnO/ZrO_2 reported by Agrell et al. will be 0.16 and 0.33 s^{-1}, respectively, at the feed of 36 $dm^3\ g^{-1}$. On the basis of the XRD pattern after the reaction in Ref. [10], we determined that the crystallite size of Cu metal for the 38 wt.% Cu/ZnO catalyst is ca. 10 nm. Assuming that all the Cu particles are spherical with a diameter of 10 nm, the surface area of the particles is calculated as 26 $m^2\ g^{-1}$ from the crystallite size. Since the Cu surface area is 20.8 $m^2\ g^{-1}$, it is estimated that most of the Cu particles are exposed. In the case of 50%Cu/ZnO, the Cu surface area is 6.2 $m^2\ g^{-1}$ and considerably smaller than the area of 16 $m^2\ g^{-1}$ calculated from the crystallite size, suggesting that the surface of Cu particles is significantly covered with other particles in comparison with the Cu particles in 38 wt.% Cu/ZnO.

The TPR profile for 38 wt.% Cu/ZnO in Ref. [10] has three peaks and the 2nd peak at ca. 190 °C is significantly larger than the 3rd peak at ca. 200 °C. This is in harmony with the discussion that most of the Cu particles are exposed in 38 wt.% Cu/ZnO, if our assignment of the TPR peaks is taken into account. Hence, it is estimated that the surface contact between Cu and ZnO particles is small and the interaction between Cu and ZnO particles in the 38-wt.% Cu/ZnO catalyst is weak in comparison with 50%Cu/ZnO; this agrees with the discussion by Günter et al. that the high surface activity is caused by the structural disorder of Cu particles which may be due to the microstrain originating from the Cu/ZnO interface [30,32]. In the case of 27 wt.% Cu/46 wt.% ZnO/32 wt.% ZrO_2 the 2nd TPR peak is larger than the 3rd peak, but the size of the 2nd peak is significantly smaller than that for 38 wt.% Cu/ZnO [10]. The TPR result suggests that the surface contact between Cu particles and ZnO and/or ZrO_2 particles for the former catalyst is larger and this accounts for the higher TOF due to the strong interaction with ZnO and/or ZrO_2 particles; no information on the Cu particle size was given for this ternary catalyst [10].

It is reported that Cu^+ species are often formed in copper supported on zirconium oxide [34,35]. Szizybalski showed the presence of Cu–O interaction in Cu/ZrO_2 reduced with hydrogen at 250 °C [14]. However, there are no significant differences in the energies of Cu $2p_{3/2}$ and Cu L_3VV between 50%Cu/ZnO and 40%Cu/ZnO/ZrO_2 reduced at 250 °C (see Figs. 10 and 11) and the surface Cu species are metallic, showing that the presence of zirconium oxide does not affect the oxidation state of the Cu surface on 40%Cu/ZnO/ZrO_2 obviously. It is considered that the interaction between Cu and ZrO_2 particles is weak in 40%Cu/ZnO/ZrO_2 and the interaction with ZnO particles is rather important. The partial agglomeration of ZrO_2 particles in the catalyst (see Fig. 5) shows that a significant part of ZrO_2 particles is not in contact with Cu particles. Thus, the higher TOF of 40%Cu/ZnO/ZrO_2 is estimated to be mainly due to the strong contact between Cu and ZnO particles.

4.3. Deactivation of the Cu catalysts during the reaction at 400 °C

The crystallite sizes of Cu and ZnO for 50%Cu/ZnO after the reaction at 400 °C for 0.5 h are significantly larger than those after the reduction at 250 °C (see Table 2), showing that the reaction at 400 °C immediately causes sintering of the catalyst despite the calcination at 500 °C for 12 h in the catalyst preparation. In general, thermally induced deactivation is caused by loss of catalytic surface area and/or chemical transformations of catalytic phases to non-catalytic phases; therefore, determination of Cu surface quantity during the reaction is important in elucidation of the deactivation process [36].

The Cu surface quantity is usually determined by the surface oxidation with N_2O, but we estimated the quantity of the catalyst after the reaction at 400 °C from the surface atomic concentrations and the BET surface area (see Table 3) due to the quantitative limitation of the catalysts recovered from the reactor [12]. The Cu surface quantity is calculated using the atomic site densities that are assumed as 0.032 mmol m^{-2} (Cu), 0.077 mmol m^{-2} (Zn^{2+}), 0.070 mmol m^{-2} (Zr^{4+}), and 0.030 mmol m^{-2} (O^{2-}) on the basis of the atomic/ionic radii. The Cu surface quantities of 50%Cu/ZnO and

40%Cu/ZnO/ZrO_2 reduced with hydrogen at 250 °C can be calculated as 0.16 and 0.21 mmol g^{-1}, respectively (see Table 3). Since the surface concentration obtained by XPS is the average of surface few layers and not that of the outermost layer, the Cu surface quantity calculated may contain the systematic error. However, the surface concentration should mainly depend on the condition of the outermost layer; thus, the Cu surface quantity calculated can be used at least for the comparison purpose within the similar system. The quantities evaluated by the oxidation with N_2O are 0.15 mmol g^{-1} and 0.17 mmol g^{-1}, respectively, showing that the evaluation from XPS and BET is fairly reliable in the present system.

The Cu surface quantity of 50%Cu/ZnO_2 after the reaction at 400 °C for 0.5 h is determined as 0.08 mmol g^{-1}, showing considerable reduction of the Cu surface quantity in comparison with the sample reduced with hydrogen at 250 °C (see Table 3). This is supported by the increase in the Cu particle size and decrease in the BET surface area (see Tables 2 and 3). Despite the steep decrease in the activity of 50%Cu/ZnO, the Cu surface quantity is almost stable during the reaction for 7 h. No significant change in the crystallite sizes of Cu and ZnO shows that the deactivation is not due to sintering (see Table 2). The change in the surface atomic concentration and decrease in the BET surface area during the reaction indicate the change in the surface structure. The stable Cu surface quantity suggests that the deactivation is mainly due to decrease in the surface activity of Cu particles. It is hypothesized that the microstrain originating from the Cu/ZnO interface is reduced by the structural change of the particles at the reaction temperature as high as 400 °C [30,32].

The Cu surface quantity for Cu/ZnO/ZrO_2 is also stable during the reaction at 400 °C (see Table 3), showing the decrease in the surface activity of Cu particles. The crystallite size of ZnO for 40%Cu/ZnO/ZrO_2 after the reaction at 400 °C for 0.5 h is the same as that just after the reduction at 250 °C while the size for 50%Cu/ZnO significant increases (see Table 2). It is considered that no significant sintering of the ZnO particles occurs in the initial stage of the reaction at 400 °C because of the presence of ZrO_2 particles. Small particles probably attributed to amorphous ZrO_2 are present with the grains attributed to Cu and ZnO (see Fig. 6). Hence, it is supposed that the small ZrO_2 particles hamper the sintering of Cu and ZnO particles. However, the increase in the crystallite sizes of Cu and ZnO after the 4th run evidences the gradual sintering of the particles during the reaction. As shown in Fig. 9, the XRD peak at 30.5° attributed to ZrO_2 gradually intensified with the time-on-stream without significant increase in the crystallite size (see Table 2), suggesting that the amorphous ZrO_2 particles undetectable by XRD crystallize gradually to XRD detectable particles (tetragonal ZrO_2) whose crystallite size is ca. 10 nm. The increase in the surface atomic concentration of Zr^{4+} implies disappearance of the ZrO_2 particles in the interface of Cu and ZnO particles (see Table 3). The crystallization is promoted in the reaction atmosphere because there is no apparent crystallization during the catalyst preparation in air at 500 °C for 12 h (see Fig. 8a).

The CO selectivity with 40%Cu/ZnO/ZrO_2 in Fig. 2 is higher than that of 50%Cu/ZnO. At the conversion of 80%, the selectivities of 40%Cu/ZnO/ZrO_2 and 50%Cu/ZnO are 3.7% and 2.5%, respectively. In the case of 30 wt.% Cu/ZrO_2 prepared by the coprecipitation method, the activity at 400 °C steeply decreases together with the crystallization of the ZrO_2 particles, while the CO selectivity increases considerably [12]. It is known that the CO selectivity produced with Cu/ZrO_2 increases with the crystallization of amorphous ZrO_2 to tetragonal phase [13]. Hence, the increase in the CO selectivity may be due to the ZrO_2 crystallization. On the contrary, the CO selectivity decreases gradually in the deactivation process of 40%Cu/ZnO/ZrO_2 (see Fig. 2), implying that the crystallization of ZrO_2 does not affect the CO selectivity. Thus, it is considered that zirconium oxide does not directly contribute to the reaction as discussed in the previous section. Matter and Ozkan reported the shift of the binding energy for Zr $3d_{5/2}$ after various pretreatments of Cu/ZnO/ZrO_2 [37]. Some surface species such as hydroxyl and formate groups can be formed on zirconium oxide in Cu/ZrO_2 [38], and this may affect the binding energy of Zr $3d_{5/2}$. However, no significant difference in the energy can be observed with the samples of 40%Cu/ZnO/ZrO_2, suggesting that the surface condition of ZrO_2 does not change significantly during the reaction at 400 °C. Hence, the deactivation mechanism of Cu/ZnO/ZrO_2 is rather close to that of Cu/ZnO while the smaller Cu particle size may retain the microstrain [32]. The gradual decrease in the activity of Cu/ZnO/ZrO_2 is probably due to the structural change in the Cu and ZnO particles accompanied with the crystallization of ZrO_2 particles. It should be noted that the crystallite size of Cu increases to 24 nm after the 4th run despite no significant change in the Cu surface quantity (see Tables 2 and 3). This suggests decrease in the surface contact between Cu particles and ZnO and/or ZrO_2 particles. The increase in the crystallite size of ZnO during the reaction may cause the decrease in the surface contact while the presence of ZrO_2 particles mitigates the deactivation process. It is considered that the structural stabilization of the ZrO_2 particles is important for the prevention of the further deactivation in the high temperature reaction.

5. Conclusions

The catalytic activity of Cu/ZnO/ZrO_2 is comparable to a commercial Cu/ZnO/Al_2O_3 in the methanol steam reforming at 250 °C. The addition of zirconium oxide to Cu/ZnO results in the higher dispersion of Cu and ZnO particles in the catalyst. After the reduction with hydrogen at 250 °C for 1 h, most of the ZrO_2 particles are amorphous and as small as 5 nm or below. Partial agglomeration of the small ZrO_2 particles can be found on the surface of the catalyst, but the major part is comprised of the mixture of the Cu and ZnO particles and the small ZrO_2 particles. The activity of Cu surface for Cu/ZnO/ZrO_2 is not significantly higher than that for Cu/ZnO. The presence of zirconium oxide does not directly affect the surface activity and it is estimated that the surface contact between Cu and ZnO particles mostly affects the high surface activity. The activity of Cu/ZnO decreases in the reaction at 400 °C, and the presence of zirconium oxide mitigates the deactivation of Cu/ZnO. No significant decrease in the Cu surface quantity can be detected, suggesting that the deactivation is mainly caused by the decrease in the surface activity in the initial stage of the reaction. The presence of the amorphous ZrO_2 particles in the aggregation of Cu and ZnO particles stabilizes the structure, and it will hamper the deactivation of Cu/ZnO caused by the decrease in the surface interaction. However, the amorphous ZrO_2 particles are gradually crystallized to the larger particles during the reaction at 400 °C and the particle sizes of Cu and ZnO are simultaneously increased. Hence, the further investigation is necessary to stabilize the structure at the high temperature, but Cu/ZnO/ZrO_2 is promising as a fundamental catalyst for the high temperature methanol steam reforming.

References

[1] S. Hočevar, W. Summers, in: A. Léon (Ed.), Hydrogen Technology, Springer, Berlin, 2008, pp. 15–79.
[2] D.R. Palo, R.A. Dagle, J.D. Holladay, Chem. Rev. 107 (2007) 3992–4021.
[3] P. Marques, N.F.P. Ribeiro, M. Schmal, D.A.G. Aranda, M.M.V.M. Souza, J. Power Sources 158 (2006) 504–508.
[4] A.F. Ghenciu, in: N. Brandon, D. Thompsett (Eds.), Fuel Cells Compendium, Elsevier, Oxford, 2005, pp. 91–106.
[5] D.G. Löffler, S.D. McDermott, C.N. Renn, J. Power Sources 114 (2003) 15–20.
[6] A. Qi, B. Peppley, K. Karan, Fuel Process. Technol. 88 (2007) 3–22.
[7] M.S. Wilson, Int. J. Hydrogen Energy 34 (2009) 2955–2964.
[8] G.C. Chinchen, P.J. Denny, J.R. Jennings, M.S. Spencer, K.C. Waugh, Appl. Catal. 36 (1988) 1–65.
[9] J.P. Green, J.R.H. Ross, Catal. Today 51 (1999) 521–533.

[10] J. Agrell, H. Birgersson, M. Boutonnet, I. Melián-Cabrera, R.M. Navarro, J.L.G. Fierro, J. Catal. 219 (2003) 389–403.
[11] P.H. Matter, D.J. Braden, U.S. Ozkan, J. Catal. 223 (2004) 340–351.
[12] Y. Matsumura, H. Ishibe, Appl. Catal. B 91 (2009) 524–532.
[13] L.-C. Wang, Q. Liu, M. Chen, Y.-M. Liu, Y. Cao, H.-Y. He, K.-N. Fan, J. Phys. Chem. C 111 (2007) 16549–16557.
[14] A. Szizybalski, F. Girgsdies, A. Rabis, Y. Wang, M. Niederberger, T. Ressler, J. Catal. 223 (2005) 297–307.
[15] .W. Evans, M.S. Wainright, A.J. Bridgewater, D.J. Young, Appl. Catal. 7 (1983) 75–83.
[16] ISO 18118, 2004.
[17] JCPDS Files, 410254, 211486, 40836, 170923, 371484, 330448, 351401, and 401037.
[18] C. Hammond, The Basics of Crystallography and Diffraction, Oxford University Press, New York, 1997, pp. 145–148.
[19] C.D. Wagner, in: D. Briggs, M.P. Seah (Eds.), Auger and X-ray Photoelectron Spectroscopy, 1, second edition, John Wiley & Sons, Inc., New York, 1990, pp. 595–634.
[20] J.W.E. Coenen, Appl. Catal. 75 (1991) 193–223.
[21] Y. Matsumura, K. Kuraoka, T. Yazawa, M. Haruta, Catal. Today 45 (1998) 191–196.
[22] I. Kasatkin, B. Kniep, t. Ressler, Phys. Chem. Chem. Phys. 9 (2007) 878–883.
[23] I. kasatkin, P. Kurr, B. Kniep, A. Trunschke, R. Schlögle, Angew. Chem. Int. Ed. 46 (2007) 7324–7327.
[24] G. Fierro, M.L. Jacono, M. Inversi, P. Porta, F. Cioci, R. Lavecchia, Appl. Catal. A 137 (1996) 327–348.
[25] C.-Z. Yao, L.-C. Wang, Y.-M. Liu, G.-S. Wu, Y. Cao, W.-L. Dai, H.-Y. He, K.-N. Fan, Appl. Catal. A 297 (2006) 151–158.
[26] F. Arena, K. Barbera, G. Italiano, G. Bonura, L. Spadaro, F. Frusteri, J. Catal. 249 (2007) 185–194.
[27] Y. Matsumura, H. Ishibe, Appl. Catal. B 86 (2009) 114–120.
[28] Y. Matsumura, H. Ishibe, J. Catal. 268 (2009) 282–289.
[29] P. Kurr, I. Kasatkin, F. Girgsdies, A. Trunschke, R. Schlögl, T. Ressler, Appl. Catal. A 348 (2008) 153–164.
[30] M.M. Günter, T. Ressler, R.E. Jentoft, B. Bems, J. Catal. 203 (2001) 133–149.
[31] G.-C. Shen, S. Fujita, S. Matsumoto, N. Takezawa, J. Mol. Catal. A 124 (1997) 123–136.
[32] B.L. Kniep, F. Girgsdies, T. Ressler, J. Catal. 236 (2005) 34–44.
[33] H. Purnama, T. Ressler, R.E. Jentoft, H. Soerijanto, R. Schlögl, R. Schomäcker, Appl. Catal. A 259 (2004) 83–94.
[34] I. Ritzkopf, S. Vukojević, C. Weidenthaler, J.-D. Grunwaldt, F. Schüth, Appl. Catal. A 302 (2006) 215–223.
[35] H. Oguchi, H. Kanai, K. Utani, Y. Matsumura, S. Imamura, Appl. Catal. A 293 (2005) 64–70.
[36] C.H. Bartholomew, Appl. Catal. A 212 (2001) 17–60.
[37] P.H. Matter, U.S. Ozkan, J. Catal. 234 (2005) 463–475.
[38] M.D. Rhodes, A.T. Bell, J. Catal. 233 (2005) 198–209.